Int. J. Electrochem. Sci., 11 **(2016)** 6799 – 6807, doi: 10.20964/2016.08.28

International Journal of
ELECTROCHEMICAL
SCIENCE
www.electrochemsci.org

Short Communication

Controllable Fabrication of $LiFePO_4$ Cathode Materials with Multiple Morphologies for Lithium Ion Batteries

Guanrao Liu, Shichao Zhang[*]*, Xin Wei, Shengbin Wang, and Yuan Yu*

School of Materials Science &Engineering, Beijing University of Aeronautics & Astronautics, Beijing 100191, China
[*]E-mail: csc@buaa.edu.cn

Received: 29 April 2016 / *Accepted:* 7 May 2016 / *Published:* 7 July 2016

Pure $LiFePO_4$ with multiple morphologies, such as nanoplate, nanocubes, and self-assembled rose-like structures, were synthesis via hydrothermal process employing surfactant CTAB as soft-template. The addition of surfactant is the key factor for controlling the crystal growth of the particles. Among these products, $LiFePO_4$ nanoplates with preferential direction of *b*-axis delivers the highest capacity at 0.1*C*, and the most stable cycle performance, indicating a great advantage of shape-control chemistry in nanomaterials preparation, and showing an enormous potential as cathode materials for high-performance lithium ion batteries.

Keywords: $LiFePO_4$, Cathode materials, Hydrothermal method, Morphology control, Lithium ion batteries.

1. INTRODUCTION

Owing to the advantages of high energy density, long cycle life and low self-discharge rate, lithium-ion batteries (LIBs) are showing great advantages for application in electric vehicles (EV) and hybrid electric vehicles (HEV). Lots of candidate cathode materials have been explored and researched to meet the requirement for the wider application of LIBs, of which the safety characteristic and lifespan should be further improved[1,2]. Among the state-of-art cathode materials, lithium iron(II) phosphate ($LiFePO_4$) with theoretical capacity of 170 $mAh \cdot g^{-1}$ is considered as one of the most promising cathode materials for LIBs [3-10], due to the advantages of long cycle life, excellent thermal stability, low cost, and environmentally benign.

$LiFePO_4$ possess an ordered-olivine structure with space group of Pnma [11], in which each FeO_6 octahedron forms zigzag planes by sharing corners, and shares edges with one PO_4 tetrahedron and two edge-shared LiO_6 octahedra. Thus $LiFePO_4$ has a very stable 3-D framework, because of the strong P-O covalent bonds in PO_4 group. The steady structure greatly reduces the risk of oxygen release and provides extreme safety during lithium intercalation/de-intercalation. However, bulk $LiFePO_4$ electrode suffers from low electronic conductivity (~10^{-9} $cm^2 \cdot s^{-1}$) and limited Li ion diffusion (~10^{-14} $cm^2 \cdot s^{-1}$) [12]. Currently, great efforts have been devoted to overcome these limitations. Obviously, nano/micro-scaled structures, which are of benefit to the transport of electrons and Li^+, offer a solution to improve the electrochemical performance of $LiFePO_4$ [13, 14]. Many methods have been proposed to fabricate $LiFePO_4$ nanomaterials, such as high temperature solid-state reaction [15, 16], spray pyrolysis [17], co-precipitation [18, 19], sol-gel method [20, 21], and hydro/solvothermal process [10, 22], etc.

With the merits of low reaction temperature, high productive rate and low cost, hydrothermal method is an effective method to obtain materials with homogeneous particle size distribution and well-defined morphologies. The nucleation and crystal growth of $LiFePO_4$ under hydrothermal condition greatly depend on parameters such as surfactant, concentration, temperature, duration and pH, etc. [23, 24]. It is generally known that Li moves along b-axis in $LiFePO_4$, and the ac-plane is active for Li^+ intercalation and de-intercalation, i.e. the electrochemical performance of nanostructured $LiFePO_4$ depends on morphology and orientation [25]. In this work, a facile hydrothermal method was reported to fabricate $LiFePO_4$ nanostructured cathode materials with multiple morphologies by adjusting the concentration of surfactant. The formation mechanisms of $LiFePO_4$ with various morphologies and the influence of surfactants on controlling crystal growth were analyzed, as well as the electrochemical properties of $LiFePO_4$.

2. EXPERIMENTAL DETAILS

2.1. Preparation of $LiFePO_4$ nanoparticles

$LiFePO_4$ nanostructures were prepared via hydrothermal process using $LiOH \cdot H_2O$, $FeSO_4 \cdot 7H_2O$ and H_3PO_4 as raw materials, which were of analytical reagents. The molar ratio of Li^+, Fe^{2+}, and PO_4^{3-} was 3:1:1. For preparation of $LiFePO_4$ nanoplates (marked as Sample-02), a typical process is as follows, 1g $FeSO_4 \cdot 7H_2O$ was dissolved in 30 mL distilled water with continuous bubbling pure N_2. Then, 0.46g H_3PO_4 (85 wt%) and cetyltrimethyl ammonium bromide (CTAB) were added into the solution (the final concentration of CTAB in reaction system was 0.016 $mol \cdot L^{-1}$). Subsequently, 4 mL LiOH solution (3 $mol \cdot L^{-1}$) was added into the solution dropwisely under stiring, and then a gray suspension was formed. The mixtures was then transfered into a Teflon-lined stainless steel autoclave with capacity of 80%. The autoclaves were sealed and for a hydrothermal reaction at 180℃ for 4h. The final products were washed thoroughly with distilled water and ethanol, and dried at 60 ℃ for 12h in a vacuum oven. $LiFePO_4$ particles with other morphologies were obtained using same route by controlling the addition of CTAB.

2.2. Structure and Morphology Characterization

X-ray powder diffraction (XRD) was employed at room temperature to investigate the crystallographic structure using a Rigaku D/MAX 2000 PC diffractormeter with a non-monochromated Cu-Kα X-ray source (λ=1.5406Å). The morphology and structure of prepared samples were observed by transmission electron microscopy (TEM) images recorded with JEOL-2100F at an acceleration voltage of 200 kV， and scanning electron microscopy (SEM) images recorded by Apollo 300.

2.3. Electrochemical measurements

Electrochemical performance of the prepared samples was measured using Swagelok-type two-electrode cells The working electrodes were pressed with a mixture of 75 wt.% active materials, 15 wt.% carbon black and 10 wt.% of polyvinylidene fluoride (PVDF) binders. Then, the prepared electrodes were dehydrated by a vacuum dry at 60℃ for 15 h and were cooled down to room temperature. The cells were integrated in an Ar-filled glove box (MB-10-G with TP170b/mono, MBRAUN) employing lithium disk as counter and reference electrodes. The electrolyte was 1M $LiPF_6$ dissolved in ethylene carbonate (EC) and dimethyl carbonate (DMC) with a volume ratio of 1:1. Celgard 2300 membrane served as separator. The galvanostatical charging/discharging measurement was performed using a battery test system (NEWARE BTS-610, Neware Technology Co., Ltd., China) with a cut-off voltage of 2.5V-4.2V (vs. Li/Li^+) at ambient temperature.

3. RESULT AND DISCUSSION

3.1. Structures and Morphologies Analysis

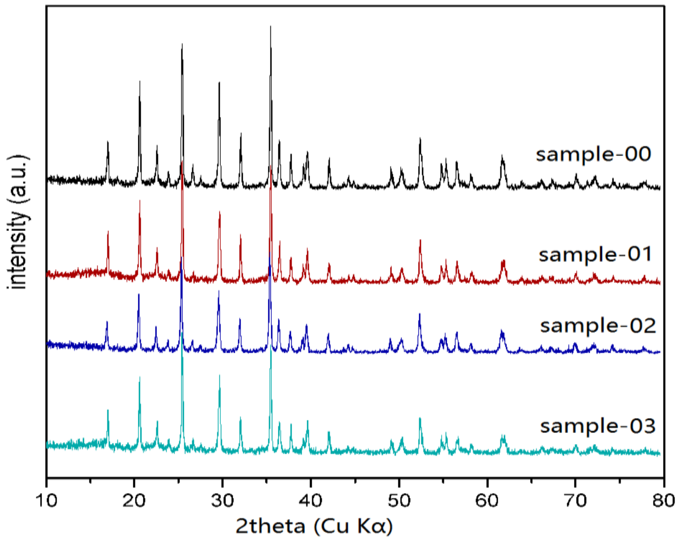

Figure 1. XRD patterns of the $LiFePO_4$ nanoparticles prepared with different concentration of CTAB. (Sample-00, without CTAB; Sample-01, 0.016M; Sample-02, 0.04M; and Sample-03, 0.08M)

The samples prepared with different amount of CTAB are list in Table 1. XRD measurements were conducted in order to investigate the crystalline properties of the prepared samples. As shown in Figure 1, all the diffraction peaks for the prepared samples can be indexed as pure olivine structure with orthorhombic Pnma space group, and no second phase were detected, which indicates the addition of CTAB has no effect on the phase of $LiFePO_4$ and does not generate impurities. The particle size was estimated by Sherrer formula, indicating that Sample-01, Sample-02, and Sample-03 are with smaller size than Sample-00, which means the sizes of particles were limited by CTAB, as well as the lattice constant.

Table 1. The structure parameters of samples prepared with different concentration of CTAB

	The concentration of CTAB / mol·L^{-1}	**a**	**b**	**c**	**a/c**
Sample-00	0.0	10.3286	6.0188	4.7030	2.1962
Sample-01	0.016	10.3821	6.01376	4.7154	2.2018
Sample-02	0.04	10.3609	6.0146	4.7090	2.2002
Sample-03	0.08	10.3201	5.9982	4.7105	2.1909

Figure 2 depicts the SEM and TEM images to identify the size and morphology of $LiFePO_4$ particles. As is shown in Figure.2a, the morphology of Sample-00 was agglomerated octahedron particles with size distribution from 500 nm to 1μm, which is not uniform enough. Figure 2b to 2e, illustrate that the addition of CTAB controlled the crystal growth and product morphologies, i.e. the size and morphologies of prepared $LiFePO_4$ particles changed with the concentration of surfactant. With addition of 0.016M CTAB, Sample-01 exhibits a plate-architecture with thickness of 200nm. When the concentration of CTAB increases to 0.04M, the obtained Sample-02 presented as smaller nanocubes with size of ~200nm (Figure 2c). It can be seen from Figure 2f that Sample-03 was with micro-roselike morphology assembled by nanorods growing radially from the center. Further structures investigations for the nanoplates (Sample-01) were directed by TEM and HRTEM. As shown in Fig.2e and f, the set of lattice fringes is clear. The interplanar spacing of 1.03 nm correspond to the d-value of (100) plane, indicating that the plate-like $LiFePO_4$ presents a preferred growth within the ac plane, which facilitates the transport of Li^+ along the *b* axis direction [25].

The formation of $LiFePO_4$ with various morphology is attributed to the self-assembly process using surfactant CTAB served as soft-template. To further understand the effects of CTAB on the crystal growth and crystalline orientation of $LiFePO_4$, several schematic illustrations are presented in Figure 3. As is shown at the bottom of Figure 3, CTAB is a kind of cationic surfactant, which can ionized completely in water, resulted in the cation CTA^+ with along alkyl tail. Compared to (100) planes, the number of nearest O on (010) plane is the most, thus CTA^+ prefers to be adsorbed on the (010) plane because of the electrostatic interaction [26]. Therefore, compared to the blank sample with octahedron structures, different morphologies were produced with the addition of CTAB. Being prepared with low concentration of CTAB, Sample-01 presents highly ordered plate architectures, owing to the absorption of CTAB on (010) planes, on which the *b*-axis direction of the crystal growth was suppressed. When the amount of CTAB gradually increasing, the nuclei will be trapped by the CTAB molecule, which prevents the crystal growth of $LiFePO_4$, and nanocubes were obtained. When the concentration of CTAB is up to form a large amount of micelles, the small $LiFePO_4$ crystals were trapped and the crystal growth was suppressed temporarily.

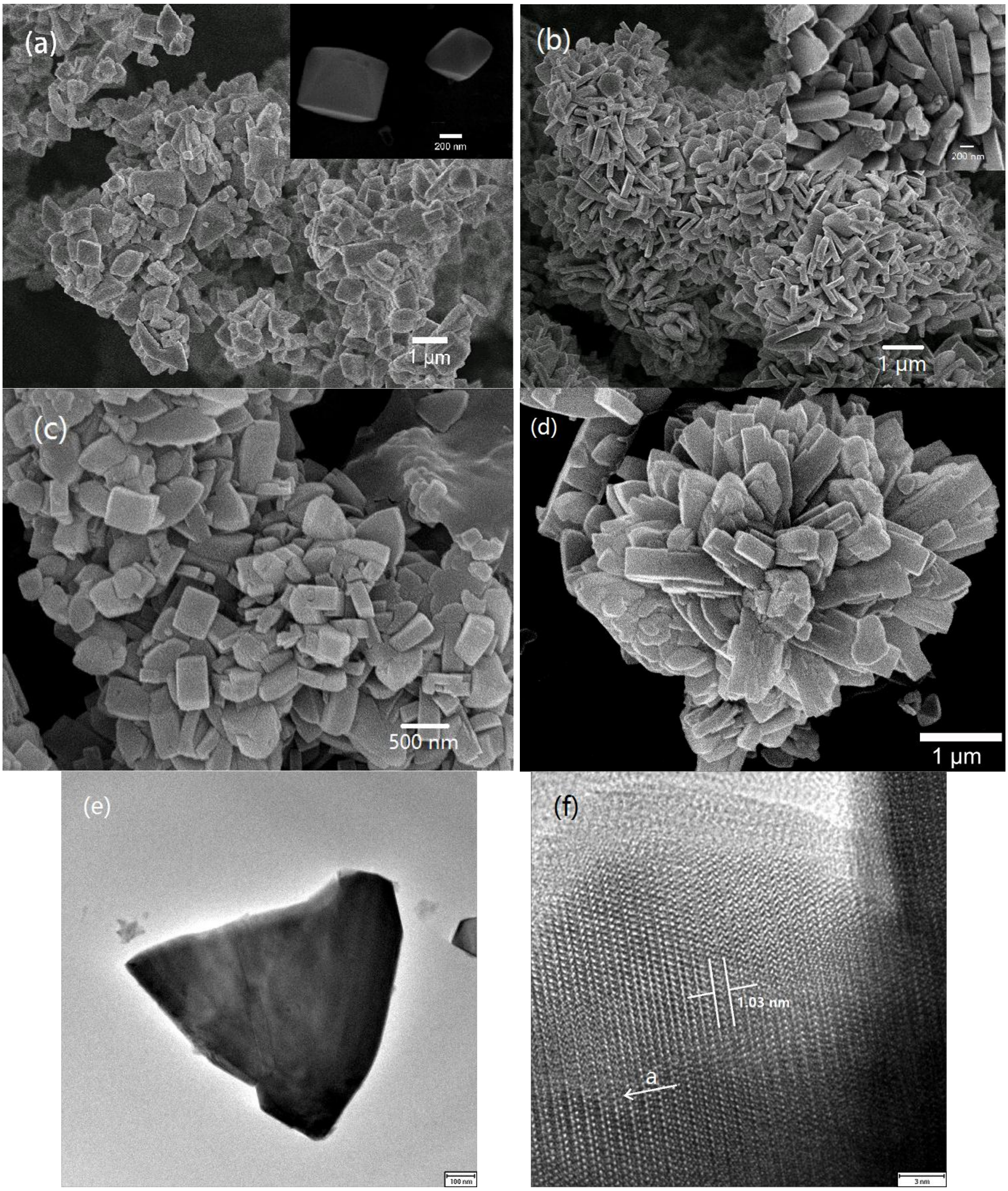

Figure 2. SEM images of (a) blank Sample-00; (b) Sample-01, (c) Sample-02 and (d) Sample-03; (e) and (f) TEM images of Sample-01

However, due to the continous ions supply from the reaction system, the crystals grow radially from the nuclei via Ostwald ripening process (smaller crystals dissolved and then regrow into larger crystals) and break the barrier of micelles. Therefore, self-assembled roselike $LiFePO_4$ secondary particles were formed (Sample-03).

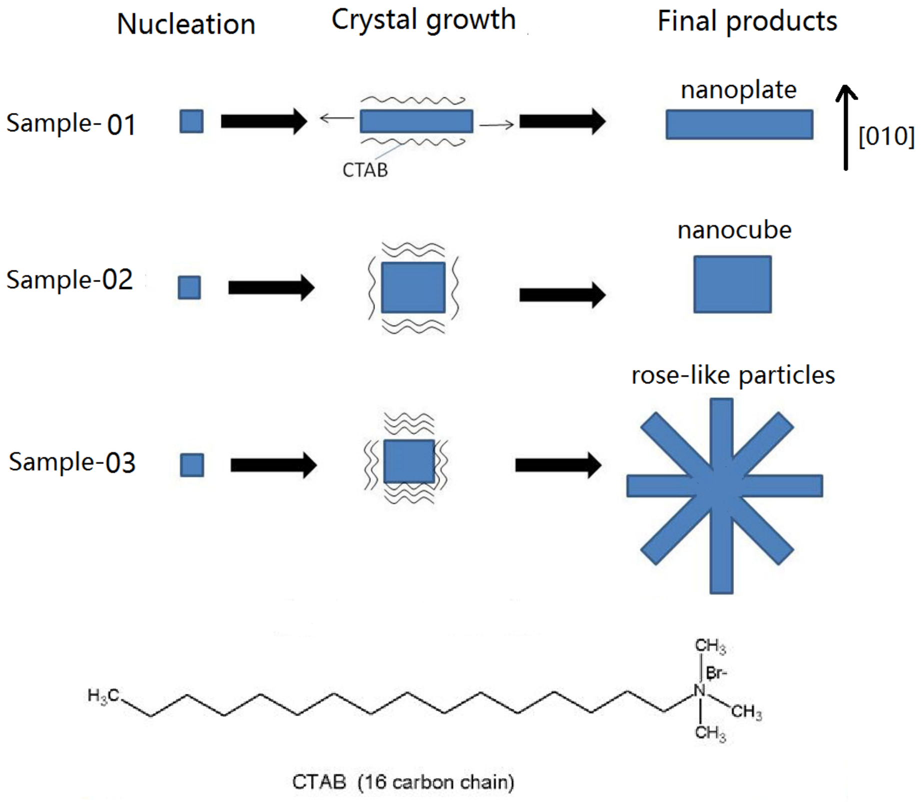

Figure 3. Schematic illusion of the formation mechanism of $LiFePO_4$ particles.

3.2. Electrochemical performances of the prepared $LiFePO_4$

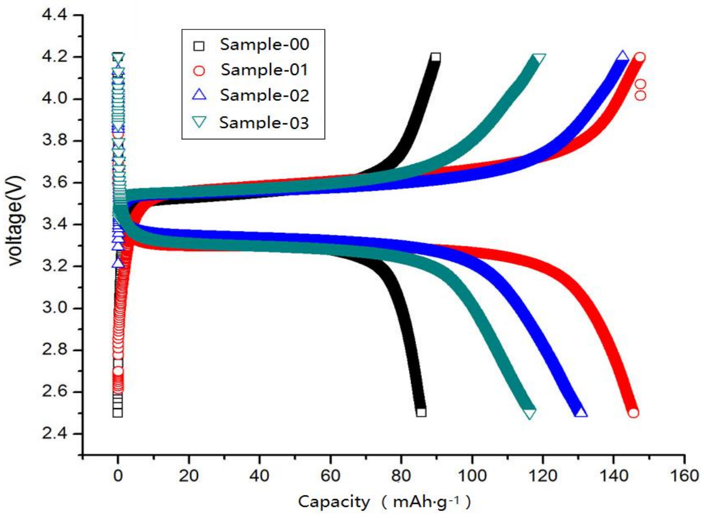

Figure 4. Initial charge-discharge profiles of the samples.

With purpose of investigating the influence of the size and shape of the $LiFePO_4$ particles on their electrochemical performance, galvanostatic charge-discharge profiles at 0.1*C* of all the prepared samples were compared as shown in Figure 4. All the samples exhibit flat potential plateaus both on charge and discharge process corresponding to the typical Li^+ intercalation/de-intercalation in $LiFePO_4$ [4]. Sample-00 prepared without any surfactant delivered the lowest discharge capacity of 86.10 $mAh{\cdot}g^{-1}$, and the highest capacity of 146.2 $mAh{\cdot}g^{-1}$ was obtained by Sample-01 with plate-architecture. It was reported that the electrochemical performance of the samples is relevant to the lattice constants of the crystals. In particular, a large value of *a/c* will contribute to a high capacity for electrode materials [27]. As is shown in Table 1, the octahedral structured Sample-00 exhibit the lower value of *a/c*, compared with Sample-01 and Sample-02. In addition, the lattice constants are also influenced by the crystallinity of the materials [28]. XRD patterns showed that the rose-like Sample-03 possessed the lowest crystallinity, due to the highest concentration of CTAB. Hence, Sample-01 was with the highest capacity because of its balance between the crystal structure and the crystallinity.

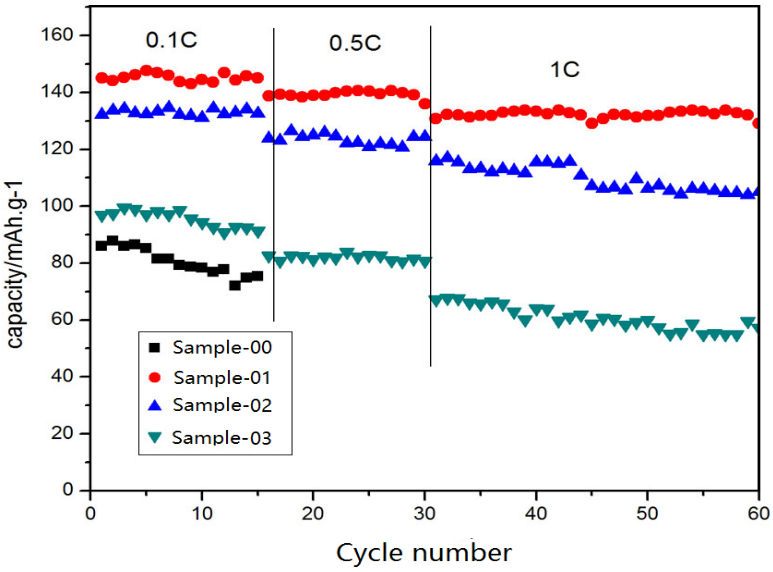

Figure 5. The rate and cycling performances of all the samples.

It is important for electrode materials providing excellent cycling stability and rate performance. As shown in Figure 5, the prepared $LiFePO_4$ samples were cycled at 2.5 ~ 4.2 V vs. Li/Li^+ with various rates (0.1*C*, 0.5*C* and 1*C*, repectively). When being cycled at low rate (<0.5*C*), all samples except for Sample-00 exhibit a stable cycle performance. It was noticed that the cycle of Sample-00 was terminated with dramatically capacity fading after 15 cycles at 0.1*C*, owing to its big size of particles resulted in a poor electron conductivity and the ability of Li^+ diffusion. At the rate of 1*C*, Sample-01 showed a discharge capacity of 130.80 $mAh{\cdot}g^{-1}$ with barely fading, while the capacities of Sample-02 and Sample-03 significantly declined after 30 cycles with capacity rentenions of 90.6% and 84%, respectively. Obviously, Sample-01 possess the most stable electrochemical performance among these samples. Smaller sized nanocubes (Sample-02) presented worse performance than Sample-01, probably owing to its poor crystallinity. As to self-assembled roselike structured Sample-03, the radial structrure from surface to center prolong the distance of Li+ ions diffusion, which affected the speed of Li^+ ions insertion and extraction. Moreover, the active materials deep in the center of the “rose” may not particepate the reation, owing to the infiltration degree of electrolyte. The excellent rate performance of Sample-01 is mainly attributed to the specific nano-plate structures with certain orientation, which reduce the distance of Li^+ diffusion and electron transport, as well as improve the immersion of electrolyte.

4. CONCLUSIONS

In summary, pure phase $LiFePO_4$ particles with various morphologies, such as octahedrons, nanoplate, nanocubes, and self-assembled roselike particles, were successfuly prepared by hydrothermal process by adjusting the concentration of CTAB, which was the key factor of controlling the crystal growth. Electrochemical performance were found to crucially depend on the structure of the products. Among these products, $LiFePO_4$ nanoplate exhibit flat potential plateaus both on charge and discharge process, and the capacity of 146.20 $mAh{\cdot}g^{-1}$ at 0.1*C*, as well as the most stable cycling performance, especially in high rate (1*C*), owing to its plate-like structures in ab-plane, which is benefit for electron transport and Li^+ ions diffusion. The facile synthesis of $LiFePO_4$ nanomaterials by controlling its crytal growth provides a effective way to achieve high-quality cathode materials.

ACKNOWLEGEMENT
The authors are grateful for the financial support from National Basic Research Program of China (973 Program) (2013CB934001) , National 863 Program of China (2013AA050904), and International S&T Cooperation Program of China (2012DFR60530).

References

1. J. Tollefson, *Nature*, 456 (2008)436
2. J. B. Goodenough, and Y. Kim, *Chem. Mater.*, 22 (2009) 587.
3. A. K. Padhi, K. S. Nanjundaswamy and J.B. Goodenough, *J. Electrochem. Soc.*, 144 (1997) 1188.
4. A. S. Andersson, B. Kalska, L. Haggstrom and J. O. Thomas, *Sol. Stat. Ionics*, 130 (2000) 41.
5. P. Subramanya Herle, B. Ellis, N. Coombs, and L. F. Nazar, *Nat. Mater.*, 3 (2004)147.
6. M. Konarova, and I. Taniguchi, *J. Power Sources*, 195 (2010) 3661.
7. J. Liu, M. N. Banis, Q. Sun, A. Lushington, R. Y. Li, T. K. Sham, and X. L. Sun, *Adv. Mater.*, 26(2014)6472.
8. L. M. Guo, Y. L. Zhang, J. W. Wang, L. P. Ma, S. C. Ma, Y. T. Zhang, E. K. Wang, Y. J. Bi, D. Y. Wang, W. C. McKee, Y. Xu, J. T. Chen, Q. H. Zhang, C. W. Nan, L. Gu, P. G. Bruce, and Z. Q. Peng, *Nat. Comm.*, 6(2015)7898.
9. X. Y. Zhang, M. van Hulzen, D. P. Singh, A. Brownrigg, J. P. Wright, N. H. van Dijk, and M. Wagemaker, *Nat. Comm.*, 6(2015)8333.
10. Z. J. Li, Z. Z. Peng, H. Zhang, T. Hu, M. M. Hu, K. J. Zhu, and X. H. Wang, *Nano Lett.*, 16(2016)795.
11. L. X. Yuan, Z. H. Wang, W. X. Zhang, X. L. Hu, J. T. Chen, Y. H. Huang, and J. B. Goodenough, *Energ. Environ. Sci.*, 4 (2011) 269.
12. B. L. Ellis, K. T. Lee and L. F. Nazar, *Chem. Mater.*, 22(2010) 691.
13. P. G. Bruce, B. Scrosati, and J. M. Tarascon, *Angew. Chem. Int. Ed.*, 47 (2008) 2930.
14. B. H. Rong, Y. W. Lu, X. W. Liu, Q. L. Chen, K. Tang, H. Z. Yang, X. Y. Wu, F. Shen, Y. B.

Chen, Y. F. Tang, and Y. F. Chen, *Nano Energ.*, 6 (2014) 173.
15. X. S. Zhang, M. Y. Huang, J. J. Huang, C. F. Yang, M. L. Qian, and S. C. Han, *Mater. Chem. Phys.*, 167 (2015) 253.
16. P. P. Prosini, M. Carewska, and M. Pasquali, *Sol. Stat. Ionics*, 286 (2016) 66.
17. W. B. Luo, L. Wen, H. Z. Luo, R. S. Song, Y. C. Zhai, C. Liu, and F. Li, *New Carbon Mater.*, 29(2014)287.
18. N. B. Bai, H. Chen, W. Zhou, K. X. Xiang, Y. L. Zhang, C. L. Li, and H. Y. Lu, *Electrochim. Acta*, 167(2015)172.
19. C. C. Huang, D. S. Ai, L. Wang, and X. M. He, *Int. J. Electrochem. Sci.*, 11(2016)754.
20. S. X. Liu, H. B. Yin, H. B. Wang, and H. Wang, *J. Nanosci. Nanotech.*, 14(2014)7060.
21. M. Chen, L. L. Shao, H. B. Yang, Q. Y. Zhao, and Z. Y. Yuan, *Electrochim. Acta.*, 168(2015)59.
22. Z. Y. Chen, M. Xu, B. L. Du, H. L. Zhu, T. Xie, and W. H. Wang, *J. Power Sources*, 272(2014)837.
23. S. F. Yang, Y. P. Zavalij, and M. S. Whittingham, *Electrochem. Commun.*, 3(2001) 505.
24. L. Wang, W. Sun, X. Tang, X. Huang, X. He, J. Li,Q.Zhang, J. Gao, G. Tian, and S. Fan, *J. Power Sources*, 244 (2013)94.
25. C.A. Fisher, and M.S. Islam, *J. Mater. Chem.*, 18 (2008) 1209.
26. W. Li, Z. Q. Wei, L. W. Huang, D. Zhu, and Y. G. Chen, *J. Alloys Compd.*, 651 (2015) 34.
27. Y. Z. Dong, Y. M. Zhao, and H. Duan, *J. Sol. Stat. Electrochem.*, 14 (2010)131.
28. T. H. Cho, and H. T. Chung, *J. Power Sources*, 14(2004) 1131.